A&A 388, 504–517 (2002)
DOI: 10.1051/0004-6361:20020413

Astronomy & Astrophysics

On the nature of variations in the T Tauri star WY Arietis (LkHα 264)

J. F. Gameiro[1,2], D. F. M. Folha[1], and V. M. Costa[1,3]

[1] Centro de Astrofísica da Universidade do Porto, Rua das Estrelas, Porto 4150, Portugal
[2] Departamento de Matemática Aplicada, Faculdade de Ciências da Universidade do Porto, Portugal
[3] Departamento de Matemática, Instituto Superior de Engenharia do Porto, Portugal

Received 12 December 2001 / Accepted 11 March 2002

Abstract. We report optical spectroscopic and photometric results from our long-term study of the T Tauri star WY Arietis (LkHα 264). The data gathered show different types of variability: variations in the continuum level, in the emission line fluxes and line profiles. The timescales associated with these variations appear quite diverse. The correlation found between the variations observed in the veiling and in the continuum flux strongly suggest that an extra continuum source veiling the stellar photospheric spectrum is the cause driving the continuum variability. The present work also unveils the presence of an accretion flow onto the star, as revealed by the O I λ7773 Å and λ8446 Å line profiles, which is the first unambiguous model-independent detection of such an event in this star. Our photometric data allowed us to find a period of 3.04 days for this star, somewhat in tune with Fernandez & Eiroa (1996). However, due to the poor time sampling our finding should be taken as tentative. A detailed analysis of the broad and narrow components of the He I line profiles indicates the presence of a hot wind during the November 1993 observation while in October 1999 a wind is only revealed by the blue wing asymmetry of the observed Balmer and CaII infrared triplet line profiles. The correlation between the strength of the hot wind and the amount of flux in the emission lines led also to the conclusion that this type of wind provides a significant contribution to the hydrogen and metal emission lines. We have also witnessed an exceptional activity during one of the nights which may be attributed to an increase in LkHα 264's accretion rate or to a flare-like event. Although it is not possible to clearly distinguish between these possibilities, the available data set points towards variable accretion as being responsible for the observed event.

Key words. stars: formation – stars: pre-main sequence – stars: individual: WY Arietis

1. Introduction

T Tauri stars (TTS) are low-mass pre-main sequence objects. Based on the strength of the Hα line they are divided into Classical TTS (CTTS) and Weak TTS (WTTS). The former display a very rich spectrum of emission lines, which was early recognised to resemble the solar chromospheric spectrum (Joy 1945).

Common to most CTTS, is a substantial non-stellar contribution to the continuum, observed from the ultraviolet to the infrared. The infrared and near-infrared excess is thought to originate in a circumstellar disk (e.g. Kenyon et al. 1994; Meyer et al. 1997). The origin of the excess observed in the optical and UV is still an open debate. Lynden-Bell & Pringle (1974) were the first to suggest that steady accretion through a boundary layer at the stellar disk interface might account for the observed excess. Many authors developed models and added lines of evidence to such a scenario (e.g. Bertout et al. 1988; Basri & Bertout 1989). Despite the initial success of this model in explaining some of the observed features, it was quickly recognised that some properties could not be accounted for (e.g. Edwards et al. 1994). A different interpretation emerged, the magnetospheric accretion scenario, which is now becoming the widely accepted paradigm. In this picture, the mass infall is channelled by strong magnetic dipolar fields and an accretion shock forms where material hits the stellar surface (Königl 1991; Camenzind 1990; Shu et al. 1994; Pearson & King 1995). The excess optical and UV continuum emission is attributed to hot spots in the stellar photosphere that result from the accretion shock(s) (Kenyon et al. 1994). Irregular brightness variations, very common in TTS, have been explained by irregular accretion and rotational modulation. Variability of emission lines could be caused by blobs of gas flowing through the magnetosphere. Gullbring et al. (1998, 2000)

Send offprint requests to: J. F. Gameiro,
e-mail: jgameiro@astro.up.pt

and Calvet & Gullbring (1998) – hereafter CG98 – have derived the amount of optical and UV excess for a sample of CTTS assuming a magnestospheric infall model. These authors have made detailed calculations of the structure of the accretion shock in CTTS and compared the derived emergent spectrum with observations. While the results are very promising, not all CTTS fit into this scheme. In fact, it is possible that for a given CTTS, at a given time in its evolution, several mechanisms are responsible for the observed activity.

In this context, we present in this paper a study of the CTTS WY Arietis (LkHα 264). This star displays most of the properties attributed to the CTTS class, has an optical spectrum typical for a K5 dwarf and an apparent magnitude $m_v \approx 12$ (Herbig & Bell 1988). LkHα 264 is associated with the MBM 12 dark cloud, with a commonly referenced distance of 65 pc (Hobbs et al. 1986). However, Luhman (2001) revise the cloud distance to 275 pc. Interferometric observations at 2.7 mm are reported by Pound (1996) but only upper limits for the flux are given. This lack of detection suggests that the disk that surrounds this star must be very tenuous. Recently, based on mid-infrared observations, Jayawardhana et al. (2001) report the presence of an optically thick disk surrounding LkHα 264.

This star also presents a blue excess emission at optical wavelengths and a Balmer jump (Valenti et al. 1993). The optical continuum of LkHα 264 has been interpreted by Valenti et al. (1993) in the context of a boundary layer model and more recently, by Costa et al. (1999) as an analogue of the Sun with a much higher level of activity. By combining UV and optical data the latter authors find that the continuum could be well fit, from 1200 Å to 7000 Å by free-free and free-bound emission from a hot dense gas plus blackbody emission at two different temperatures, one related to the stellar spectral class and the other associated to an hot spot covering a small fraction of the stellar surface.

Gameiro et al. (1993) present UV and optical spectroscopic observations of LkHα 264. In their work, time series of high resolution optical spectra for the regions of the Hα, He I λ5876 Å and Na I D lines are reported. In a later work Lago & Gameiro (1998) show time-series analysis of high-resolution profiles of the same lines. In this case, the authors claim to find correlations in the behaviour of the equivalent widths of He I and Na I D which holds for timescales of 1 day down to 1 hour. However, this correlation apparently breaks down for timescales of ≈20 min.

In this paper we present optical spectroscopic and photometric observations of LkHα 264 and discuss the observed variability. In Sect. 2 we describe the observations and the data reduction. Section 3 is dedicated to the analysis of the spectroscopic properties of the star in terms of continuum and emission lines. Differential photometry data are shown in Sect. 4. A detailed discussion follows in Sect. 5 and we close with general conclusions in Sect. 6.

Table 1. Log of spectroscopic observations. Columns 1 to 2 and 4 are self explanatory. Column 3 specifies the band of the observation: Hα corresponds to IDS data centred at 6560 Å and He I+Na D to IDS data centred at 5880 Å, *low* to IDS low resolution data, *blue* to ISIS blue arm data and *red1* and *red2* to ISIS red arm data.

Date	JD-2 449 000	band	T_{exp} (sec.)
1993 Nov. 26	318.43	Hα	1000
1993 Nov. 26	318.44	He I + Na D	1000
1993 Nov. 26	318.50	Hα	1000
1993 Nov. 26	318.51	He I + Na D	1000
1993 Nov. 26	318.53	He I + Na D	1000
1993 Nov. 26	318.54	Hα	1000
1993 Nov. 26	318.60	He I + Na D	1000
1993 Nov. 26	318.62	Hα	1000
1993 Nov. 26	318.63	low	200
1993 Nov. 26	"	low	200
1993 Nov. 28	320.34	Hα	1000
1993 Nov. 28	320.55	Hα	1000
1993 Nov. 28	320.56	He I + Na D	1000
1993 Nov. 28	320.36	low	200
1993 Nov. 29	321.36	low	200
1993 Nov. 29	321.51	He I + Na D	1000
1993 Nov. 29	321.60	Hα	1000
1993 Nov. 29	321.62	He I + Na D	1000
1993 Nov. 29	322.44	He I + Na D	1000
1993 Nov. 29	322.46	Hα	1000
1993 Nov. 30	322.54	low	200
1999 Jul. 27	2386.5	blue	240
1999 Jul. 27	2386.5	red1	120
1999 Jul. 27	2386.5	red2	120
1999 Oct. 19	2470.7	-	900
1999 Oct. 21	2472.5	low	1200

2. Observations & data reduction

The observations discussed here were obtained with the Isaac Newton Telescope (INT), the William Herschel Telescope (WHT) and the Jacobus Kapteyn Telescope (JKT), at the La Palma Observatory. INT spectroscopic observations were carried out from 1993 November 26 to 30 and in 1999 October 21. WHT observations were done during the night of 1999 July 27 with ISIS and during the night of 1999 October 19 with UES. JKT differential photometry was obtained from 1999 September 13 to 18 and from 1999 October 3 to 6.

The INT Intermediate Dispersion Spectrograph (IDS) was used with the 500-mm camera plus a EEV5 400×1280 pixels CCD in 1993. Two gratings, 1800 and 150 lines/mm, were used giving different resolutions and spectral coverages. As determined from the *FWHM* of arc spectrum lines, the resolutions obtained were 0.4 and 4.5 Å respectively. The higher resolution spectra (grating of 1800 lines/mm) were centred at 5880 Å and 6560 Å and cover a band 240 Å wide. The lower resolution spectra cover the wavelength range from 3800 Å to 7000 Å.

The ISIS spectrograph at the WHT was used to obtain spectra covering the wavelength range between 3020

and 8040 Å. This coverage was achieved by obtaining one spectrum in the ISIS blue arm and two spectra, centred at different wavelengths, in the ISIS red arm. The blue arm was setup with the R300B grating and EEV12 (2148×4200 pixels) CCD, giving a resolution of 0.86 Å per pixel. The red arm was setup with the R316R grating and TEK4 (1124×1124 pixels) CCD, providing a resolution of 0.79 Å per pixel. The three spectra were combined in order to obtain the desired wavelength coverage.

The UES was used with the E31 grating, set up a central wavelength of 6548 Å. The slit width of 1.30 arcsec and the length of 6 arcsec, provided a full spectral coverage between 4663 and 10 265 Å in a total of 66 echelle orders with $R \approx 100\,000$.

The log of the spectroscopic observations is presented in Table 1. In this table IDS high resolution data is identified by "Hα" or "He I+Na D" respectively if centred at 6560 Å or 5880 Å, IDS low resolution data is identified by "low", ISIS data is identified by "blue", "red1" and "red2".

The spectral reduction was standard including background subtraction, flat-fielding with a tungsten lamp, removal of cosmic rays and wavelength calibration. The low resolution spectra obtained in 1993 and in 1999 were flux calibrated with the spectrophotometric standard star HD19445. The quality of the flux calibration was tested by comparing the derived values for the most stable stars in the sample with those found in the literature. This test, complemented by night to night comparison of flux standards, indicates that uncertainties in the flux calibration are less than 5% between 4000 and 7000 Å. Another estimate has been done by comparing two consecutive observations taken with a time interval of 200 s. During this short interval we can assume that the continuum variation is small and the difference in flux can be used as an estimate of the flux uncertainty. We obtain differences in the continuum flux which are less than 3% for wavelengths longer than 5500 Å but that increase towards the blue, reaching almost 15% for wavelengths shortward of 4000 Å.

The JKT was used with the JAG-CCD camera coupled to the Site2 (2048×2048 pixels) detector giving a pixel scale of 0.33 arcsec/pixel. Images were taken in two filters: Sloan g (g') and Sloan r (r'), giving an unvignetted field of view of about 8.5 arcmin diameter. The log of the *JKT* observations is presented in Table 2.

The *JKT* data was reduced following standard IRAF procedures. For each night, flat fielding was achieved from a master flat produced from sky frames obtained either in the evening and/or dawn twilight of that same night. Instrumental magnitudes for the target objects were obtained with the APPHOT package on IRAF, taking an aperture 20 pixels in radius and an annular sky aperture, centred on the star, with inner radius of 25 pixels and 5 pixels wide. The errors in instrumental magnitudes were estimated from a Poissonian noise model which takes into account the detector's read noise and gain.

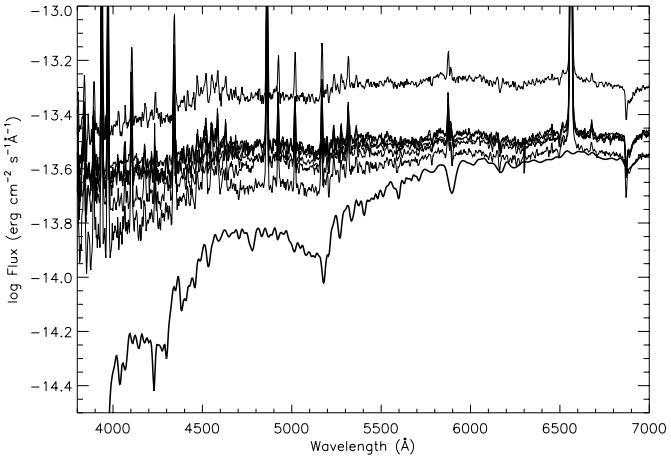

Fig. 1. Thin solid lines: LkHα 264 flux calibrated observed spectra; the uppermost spectrum was obtained on JD 2449322.54 (1993 Nov. 30). Thick solid line: photospheric contribution to the spectrum of LkHα 264 (computed as explained in Sect. 3.1).

Table 2. Log of the photometric observations. Columns are self explanatory.

Date	JD	Sloan g		Sloan r	
	$-2\,449\,000$	sec(ζ)	$T_{\rm exp}$ (s)	sec(ζ)	$T_{\rm exp}$ (s)
1999 Sep. 13	2435.63	1.061	180	1.071	60
1999 Sep. 14	2436.66	1.022	60	-	-
1999 Sep. 15	2437.73	1.046	60	1.043	40
1999 Sep. 16	2438.74	1.072	60	1.068	40
1999 Sep. 17	2439.68	1.075	60	1.071	40
1999 Sep. 18	2440.74	1.073	60	1.068	40
1999 Oct. 03	2455.75	-	-	1.269	12
1999 Oct. 04	2456.73	-	-	1.180	12
1999 Oct. 05	2457.74	1.204	50	1.220	12
1999 Oct. 06	2458.73	1.243	100	1.220	20

3. Spectroscopy

The general structure of LkHα 264's optical spectrum is similar to those of many other CTTS. The strongest lines present are those from the Balmer series, Ca II H and K and several other metallic lines dominated by Fe II, Fe I, He I, Ti II and Na I. Large Fe II blends are seen at wavelengths centred at 4200, 4600 and 5300 Å, making difficult the determination of the continuum level there. The weakness of the absorption lines indicates the presence of continuous and/or line excess emission.

3.1. The continuum

The observed low resolution spectra (flux calibrated) are shown in Fig. 1 as thin solid lines. With one exception, they cluster at continuum levels below $10^{-13.5}$ erg cm^{-2} s^{-1} Å^{-1}. The largest continuum variations are observed at shorter wavelengths.

In 1999 we had the chance to observe the star twice, in July and October. In this case, the continuum level

was similar to that observed during the 1993 run with the exception of the last night of the run (JD 2449322.54). Also, Valenti et al. (1993) and Mendoza et al. (1990) published flux calibrated spectra of this star, obtained during October 1981 and August 1989, respectively. The former extends from the Balmer jump to Hβ and the latter covers roughly the same spectral range as our own data. The continuum level in their spectra occurs at a very similar level to that observed by us in the first four nights of the 1993 run and in the 1999 spectra. This suggests that the continuum level in LkHα 264 spectra is typically below $10^{-13.5}$ erg cm^{-2} s^{-1} Å^{-1} (in the blue), with the November 30 observation catching the star in an atypical state. Applying the transmission curve for the V band to the flux calibrated spectra obtained during this atypical night and the previous one, we estimate a flux ratio of roughly 2, i.e. a variation in magnitude of 0.75 over one night. As we will show in Sect. 3.2, this increase correlates with an increase in the veiling, as measured from our IDS high resolution spectra obtained during the same nights. This correlation confirms that the flux variation does not result from errors during the flux calibration for this particular spectrum.

The low resolution spectra presented here allow us to derive the spectrum of the excess flux by assuming the shape and intensity of the stellar photosphere. The shape of the photospheric contribution of a TTS can be represented reasonably well by that of a main sequence star of the same spectral type. In this work, we have used a K5 V spectrum from the stellar spectral flux library of Pickles (1998).

The absolute level of the photospheric contribution was fixed by equating the flux near 5850 Å, obtained from the calibrated low resolution spectrum obtained at JD = 2449318.60, to the veiling at that wavelength [1], as determined from the high resolution spectrum obtained at JD = 2449318.63, i.e. data separated in time by just under 45 minutes. We reddened the photospheric spectrum using an optical extinction of $A_V = 0.8$ (Costa et al. 1999) and the Cardelli et al. (1989) reddening curve. The photospheric contribution so determined is overplotted as a solid thick line in Fig. 1. Spectra of the excess emission, determined by subtracting the photospheric contribution from the observed spectra, are shown in Fig. 2.

3.2. The veiling

The IDS high resolution spectra were used to determine the amount of veiling in LkHα 264, i.e. the ratio of the excess flux to the photospheric flux. The photospheric lines of LkHα 264 have been identified as the veiled photospheric spectrum of a K3 – K5 star and the veiling was derived using a method based on that described in Hartigan et al. (1989), which compares the spectrum of the T Tauri star with that of a template star within a small wavelength

[1] $r_\lambda = F_{\mathrm{exc},\lambda}/F_{\mathrm{phot},\lambda}$ and $F_{\mathrm{obs},\lambda} = F_{\mathrm{phot},\lambda} + F_{\mathrm{exc},\lambda}$ hence $F_{\mathrm{phot},\lambda} = F_{\mathrm{obs},\lambda}/(1 + r_\lambda)$.

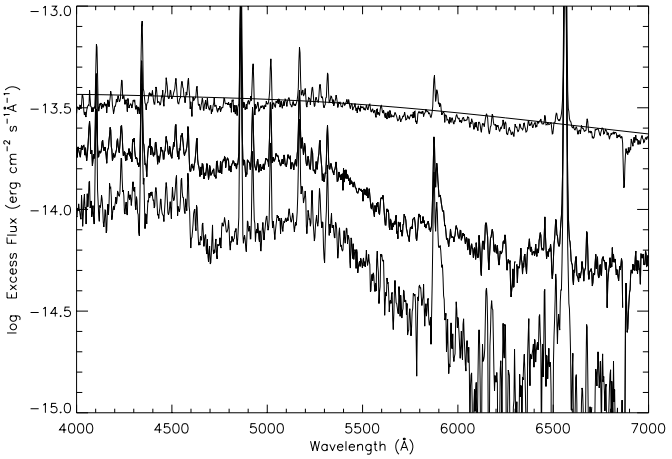

Fig. 2. Spectra of the excess flux for the nights of 1993 Nov. 30 (top), 1993 Nov. 26 (middle) and 1993 Nov. 29 (bottom). The remaining excess spectra (not shown) fall between the latter two spectra. The solid thick line represents a 8700 K black body reddened with an A_V of 0.8 and covering 6% of the stellar surface (see Sect. 5.1).

band (a few tens of Ångströms wide) and assuming the veiling to be constant in this region. We used HD 16160 (K3V) as template star, rotationally broadened to a $v \sin i$ of 20 km s^{-1}, in order to get the same blend of lines as in LkHα 264 spectrum. The veiling was computed in the regions 5910–6000 Å and 6600–6670 Å, near the He I+Na D and Hα emission lines respectively. The main photospheric lines in these regions are Fe I lines.

The night to night variations in these two bands are quite similar (Fig. 3). We should note that in comparison with veiling determinations in the He I+Na D band, the uncertainties in the veiling near Hα are significantly larger (less than 10% in the former and at times larger than 25% in the latter). This is due to the intrinsic weakness of the photospheric lines of a K3-5 dwarf near Hα, and also due to a larger uncertainty in the placement of the continuum level in this band. The latter results from the presence of very extended wings in the Hα emission line.

During the night of 1993 Nov. 26 (JD 2449318), we obtained four spectra in both bands and it is clear that the measured absolute veiling shows strong variations, the veiling varies from 0.3 to 0.5 on a time scale of hours. These variations on relatively short timescale seem to be characteristic of this star. Furthermore, during the night of 1993 Nov. 28 (JD 2449320), the veiling around the Hα region decreased by a factor of 3 in just 5 hours, suggesting large variations of the amount of excess emission on relatively short time scales.

The quasi-simultaneous observations in high and low resolution during the 1993 run allow to compare the veiling variability, as determined from the IDS high resolution spectra, with the continuum variability, as determined from the low resolution spectra. If the veiling was just an effect of continuum excess, we would expect a strong correlation between veiling and continuum flux. Since the veiling is a relative measure of the continuum excess

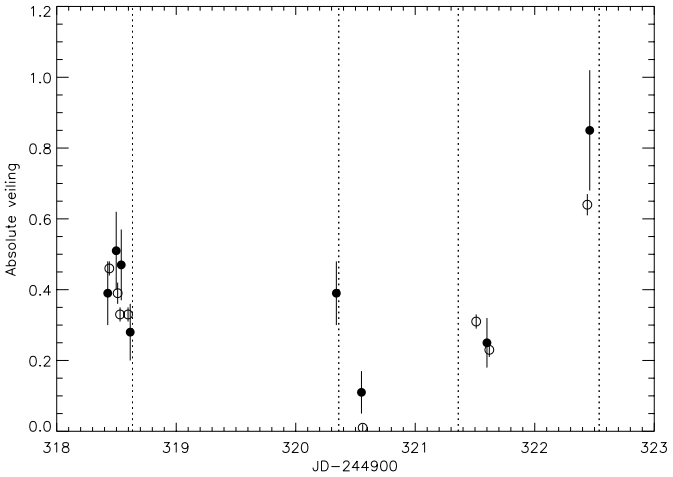

Fig. 3. The veiling level during 1993 Nov. 26-30 in the bands near the Hα (filled circles) and Na D+He I (open circles) lines. The vertical doted lines represent the instant in time when low resolution flux calibrated spectra were obtained.

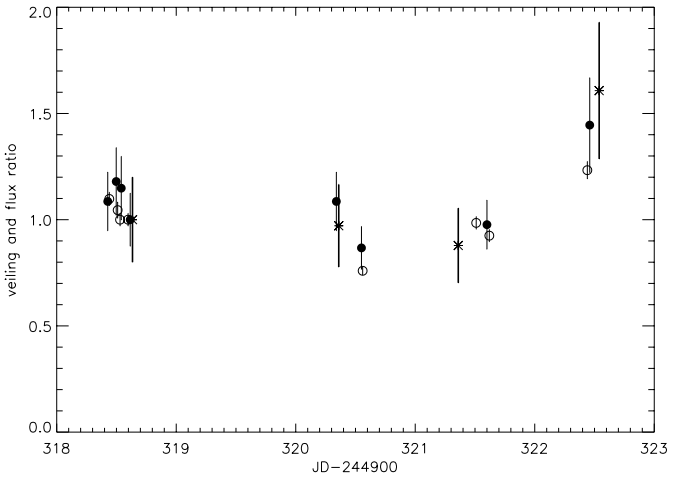

Fig. 4. Veiling ratios in the bands near the Hα (filled circle) and Na D+He I (open circles) lines and total continuum flux ratios obtained near the Hα emission line (asterisks) for the 1993 run.

(non-photospheric) flux, it cannot be directly compared to the observed continuum flux at a given wavelength. However, it is easily seen that the ratio of the observed continuum flux at a given wavelength, in two different nights i and j, $F_{\lambda,i}/F_{\lambda,j}$, is equal to the ratio $(1+r_{\lambda,i})/(1+r_{\lambda,j})$, where $r_{\lambda,i}$ and $r_{\lambda,j}$ are the veilings in nights i and j at wavelength λ.

In Fig. 4 we compare the observed continuum flux (from low resolution data) to the observed veiling (from veiling determinations). Comparisons are done in the sense described in the paragraph above with all ratios computed with respect to JD = 2449318.60 and JD = 2449318.63, respectively for continuum flux ratios and veiling ratios. Clearly the veiling and continuum ratios coincide within the error bars. This shows that indeed, the observed veiling results from an extra source of continuum, not to emission in the lines themselves.

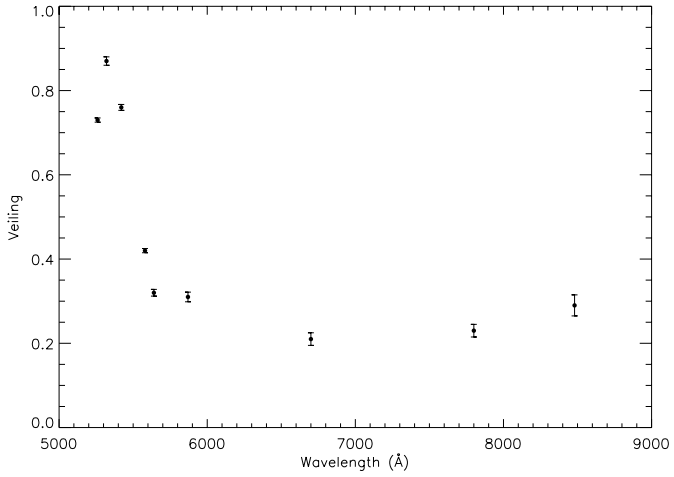

Fig. 5. Veiling variation with wavelength for JD 2451470.7 (from nine echelle orders).

The veiling was also computed from the echelle spectrum obtained on the night JD 2451470.7. In this particular spectrum it is possible to determine the veiling variation with wavelength from roughly 5200 to 8500 Å. The lower S/N at the region blueward 5000 Å and the weakness of photospheric lines for wavelengths larger than 8500 Å prevent any veiling determination in these regions. The results are plotted in Fig. 5.

The steep rise in veiling towards the blue and a smooth increase redwards 6700 Å is quite clear. The veiling near 5870 Å, i.e., near the He I and Na D lines, is 0.31 ± 0.02, and near Hα line is 0.21 ± 0.03 in good agreement with the values found at those regions during the period between JD 2449318 and 2449321. This fact is an indication that the continuum level at the time of the echelle observation (JD 2451470.7) was similar to the average continuum level observed during the 1993 run and also similar to that observed at low resolution two nights later in JD 2451472.5.

3.3. The emission lines

3.3.1. Line fluxes

In Table 3 we list the fluxes of the strongest emission lines observed in the low resolution spectra. The fluxes were obtained for each line by multiplying its equivalent width by the mean flux level of its neighbouring continuum. It should be noted that the pairs CaII H + Hϵ and He I + Na D are not fully resolved. For those lines Table 3 gives only the combined fluxes. Figure 6 displays the temporal variations of line fluxes. Due to the large time gap between the 1993 and 1999 observations, the x-axis in these figures is non-continuous. The uncertainties in fluxes are directly related to the uncertainties regarding the continuum placement and accuracy of flux calibration (see Sect. 3.1).

In order to compare the variations in the line fluxes with the variations in the continuum level we plot in Fig. 7 the continuum level near each of the emission lines. The dashed line in Fig. 7 represents the mean continuum level

Table 3. Observed fluxes of the strongest emission lines (in erg cm^{-2} s^{-1}).

JD	2449318.63	2449320.36	2449321.36	2449322.54	2451386.5	2451472.5
H8	1.02e-13	1.85e-13	1.06e-13	1.80e-13	8.1e-14	3.6e-14
Ca II K	8.64e-13	8.84e-13	6.59e-13	1.30e-12	6.50e-13	3.22e-13
Ca II H	6.47e-13	6.32e-13	4.71e-13	7.93e-13	5.5e-13	2.6e-13
Hδ	2.32e-13	2.86e-13	1.96e-13	3.21e-13	1.67e-13	5.7e-14
Hγ	3.49e-13	3.84e-13	3.e-13	4.81e-13	2.34e-13	1.26e-13
Hβ	8.10e-13	9.67e-13	7.17e-13	1.24e-12	6.33e-13	2.59e-13
Fe II (λ4924)	1.19e-13	1.46e-13	9.5e-14	1.42e-13	7.7e-14	1.9e-14
Fe II (λ5018)	1.45e-13	1.79e-13	1.07e-13	1.73e-13	8.8e-14	1.9e-14
Fe II (λ4924)	1.69e-13	2.11e-13	1.48e-13	2.31e-13	1.12e-13	2.3e-14
Fe II (λ5317)	9.8e-14	1.32e-13	8.6e-14	1.37e-13	6.5e-14	4.0e-14
He I + Na D	1.15e-13	1.33e-13	9.3e-14	1.30e-13	5.1e-14	2.6e-14
Hα	2.92e-12	3.88e-12	2.98e-12	5.51e-12	3.29e-12	-

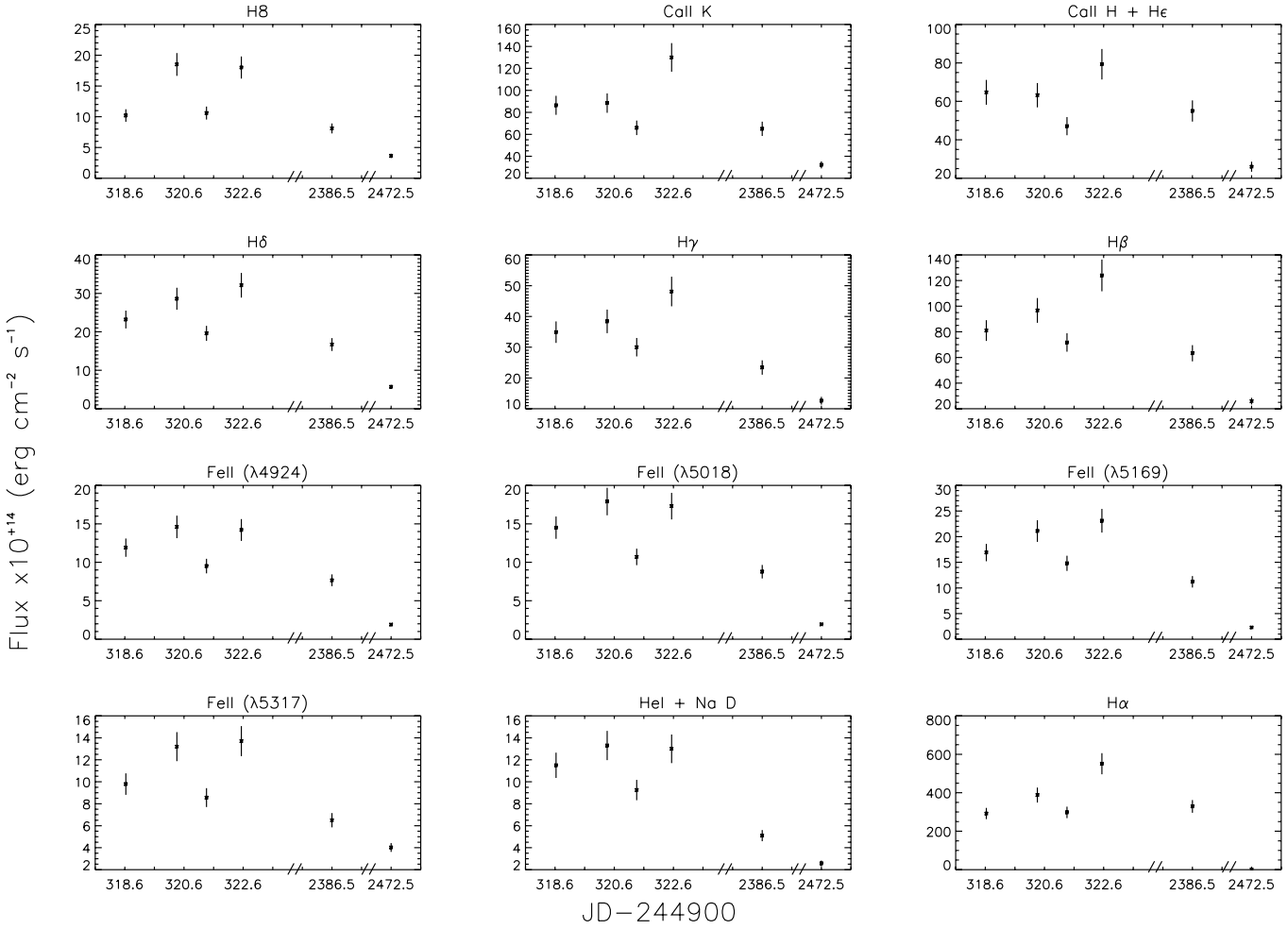

Fig. 6. Flux of the strongest emission lines observed in the low resolution spectra.

obtained by excluding the data point corresponding to JD 2449322.54, the atypically high observed continuum level. The continuum levels measured form the spectra published by Mendoza et al. (1990) and Valenti et al. (1993) are shown in Fig. 7 as solid and dotted lines, respectively. These should be regarded as rough estimates only.

As expected, Fig. 7 shows that the continuum level near the selected lines is roughly constant, with the exception of that corresponding to the spectrum observed at JD 2449322.5. Relative emission line flux variations, with respect to the mean, are larger than those observed in the continuum, with a clear decrease in flux for all the lines in the last spectrum (JD 2451472.5). In Table 4 we list the correlation coefficient of lines and lines versus their nearby continuum. It should be noted that the small number of points taken in this calculation does not allow a high confidence level. In Table 4 we represent in bold the

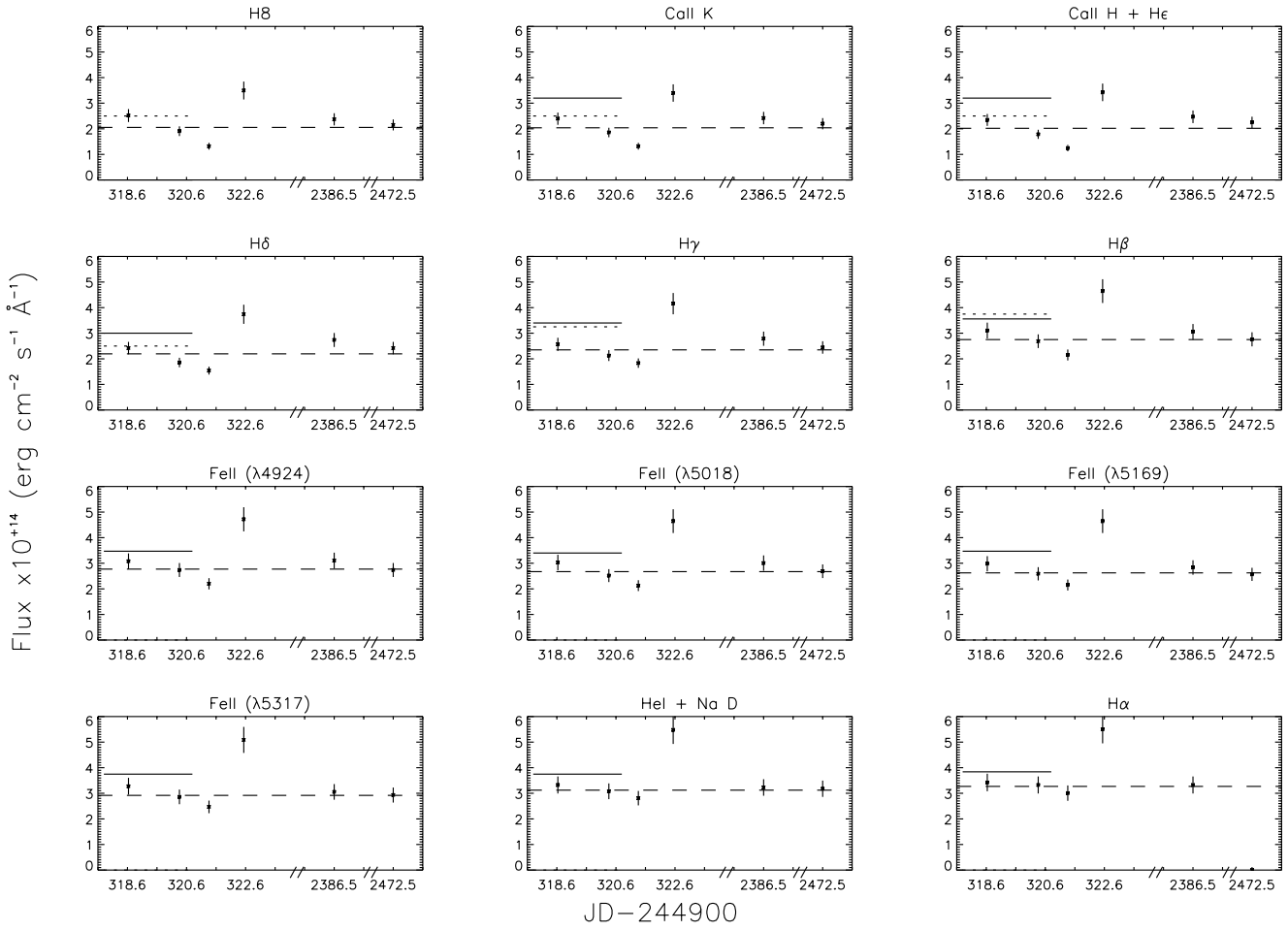

Fig. 7. Continuum level near emission lines observed in the low resolution spectra.

coefficient for which the false alarm probability is less than 0.01. The numbers suggest that, in general, the behaviour of the emission lines is well correlated.

In contrast to the correlation found in the behaviour of the emission lines amongst themselves, emission lines and continuum flux do not seem to be in general correlated. While the maximum observed flux of almost all lines occurs on the same night as the maximum continuum level, i.e. at JD 2449322.54, when we consider all nights we see no significant correlation between emission line and continuum flux (see Table 4). Hence, variations in line emission appear to be, often, decoupled from variations in the continuum.

In the particular case of JD 2449322.54, the relatively large increase in the continuum level was accompanied by an increase in the line fluxes. Although relative variations differ from line to line the observations suggest that the source producing the increase in the continuum level during this night also produced the strengthening of the emission lines.

3.3.2. He I Lines

Amongst the emission lines seen in the spectrum, the He I lines are particularly interesting, due to their high excitation potential. The lines can be formed in two ways: collisional excitation, requiring gas temperatures larger than 25 000 K, or photoionization followed by recombination and cascade, requiring local kinetic temperatures between 8 000 and 15 000 K (see Beristain et al. 2001 – hereafter BEK01– and references therein).

LkHα 264 shows He I λ5876 Å and He I λ6678 Å in emission. In addition, both lines are variable in the shape of their profiles and in their strength. Figure 8 illustrates this fact for the He I λ5876 Å line, where the line profiles observed on October 19 1999 and on November 28 1993 are shown. The He I λ6678 Å profiles (not shown) are similar in shape to those of He I λ5876 Å yet narrower and less intense. See Fig. 7 of Lago & Gameiro (1998) for the full set of He I λ5876 Å profiles obtained during the 1993 run.

According to several authors, the He I line profiles in CTTS are formed by two components (e.g. Hamann & Persson 1992; Batalha et al. 1996). A narrow component (NC), of Full Width Half Maximum (*FWHM*) typically smaller than 2 Å, whose origin is usually attributed to the post-shock region of an accretion shock and a broad component (BC), with typical *FWHM* up to around 6 Å, which is believed to contribution to line emission from a hot wind and from accreting material (see BEK01).

Table 4. Correlation coefficient of lines and lines versus continuum. The continuum in the last column is the continuum nearby the line in consideration. The value a bold mean that the false alarm probability is less than 0.01.

	H8	CaIIK	CaIIH	Hδ	Hγ	Hβ	Fe II λ4924 Å	Fe II λ5018 Å	Fe II λ5169 Å	Fe II λ5317 Å	He I	Hα	continuum
H8	**1.00**	0.87	0.83	**0.95**	**0.92**	**0.93**	**0.94**	**0.94**	**0.95**	**0.98**	**0.91**	0.77	0.31
CaIIK	0.87	**1.00**	**0.97**	**0.95**	**0.97**	**0.98**	0.89	0.89	**0.93**	**0.91**	0.86	0.91	0.61
CaIIH	0.83	**0.97**	**1.00**	**0.95**	**0.94**	**0.96**	**0.92**	**0.92**	**0.93**	0.88	0.85	0.83	0.51
Hδ	**0.95**	**0.95**	**0.95**	**1.00**	**0.99**	**0.99**	**0.99**	**0.98**	**1.00**	**0.98**	**0.95**	0.82	0.28
Hγ	**0.92**	**0.97**	**0.94**	**0.99**	**1.00**	**0.99**	**0.95**	**0.95**	**0.98**	**0.97**	**0.95**	0.82	0.50
Hβ	**0.93**	**0.98**	**0.96**	**0.99**	**0.99**	**1.00**	**0.95**	**0.94**	**0.98**	**0.96**	**0.91**	0.92	0.63
Fe II	**0.94**	0.89	**0.92**	**0.99**	**0.95**	**0.95**	**1.00**	**1.00**	**0.99**	**0.97**	**0.97**	0.63	0.41
Fe II	**0.94**	0.89	**0.92**	**0.98**	**0.95**	**0.94**	**1.00**	**1.00**	**0.99**	**0.97**	**0.98**	0.63	0.39
Fe II	**0.95**	**0.93**	**0.93**	**1.00**	**0.98**	**0.98**	**0.99**	**0.99**	**1.00**	**0.98**	**0.97**	0.77	0.52
Fe II	**0.98**	**0.91**	0.88	**0.98**	**0.97**	**0.96**	**0.97**	**0.97**	**0.98**	**1.00**	**0.97**	0.75	0.54
He I	**0.91**	0.86	0.85	**0.95**	**0.95**	**0.91**	**0.97**	**0.98**	**0.97**	**0.97**	**1.00**	0.51	0.40
Hα	0.77	0.91	0.83	0.82	0.82	0.92	0.63	0.63	0.77	0.75	0.51	**1.00**	0.98

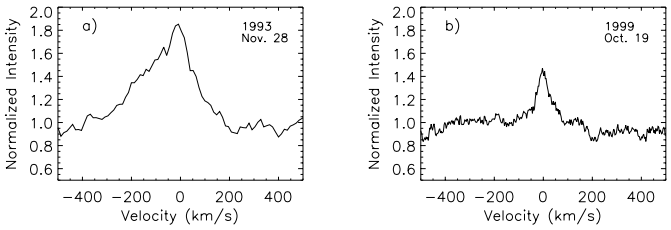

Fig. 8. He I λ5876 Å line profiles. Panel **a)** JD 2449320.56 (1993 November 28); panel **b)** JD 2451470.7 (1999 October 19). The velocity scale is in the stellar rest frame.

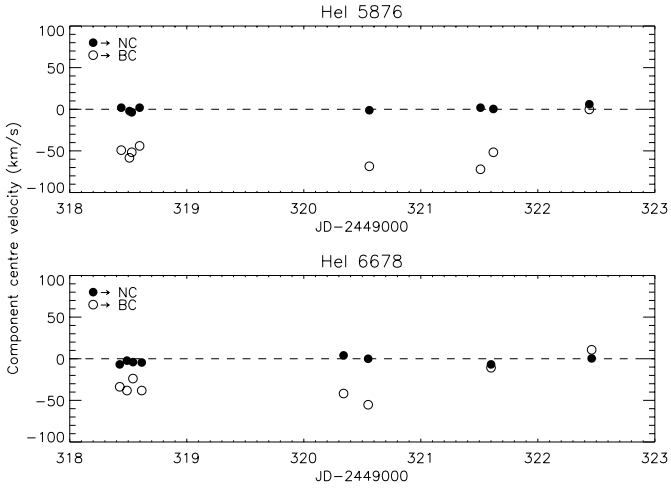

Fig. 9. Centre velocity of the He I lines narrow (NC) and broad (BC) components. Top panel: He I λ5876; Bottom panel: He I λ6678. Filled circles refer to the NC and open circles to the BC. The size of the symbols corresponds to the spectral resolution (10 km s^{-1}). Uncertainties in computed velocities are smaller than the symbol size.

Lago & Gameiro (1998) suggest that for LkHα 264 the He I λ5876 Å profile is made up of two components but did not analyse each of them quantitatively. Following the work of BEK01 we decomposed the He I λ5876 Å and λ6678 Å lines into broad and narrow components by Gaussian fitting.

The BC and NC in LkHα 264 are characterised by *FWHM* of 5.2 ± 0.4 Å and 1.3 ± 0.06 Å respectively. Figure 9 shows the centre velocity of each component for both lines. Uncertainties in the computation of these velocities are smaller than 10 km s^{-1}, which is the spectral resolution of the data.

The NCs in LkHα 264's He I profiles peak near the stellar rest velocity, with no significant shift between the He I λ5876 and He I λ6678 NCs. In contrast, the BCs of the He I lines tend to be slightly blueshifted, between 50 and 80 km s^{-1} for He I λ5876 and up to about 60 km s^{-1} for He I λ6678. An exception to this behaviour occurs in the night JD 2449322.54, when the BCs of both lines peak near zero velocity (see Fig. 9). Hence, the state of high continuum level observed during that night is accompanied by a clear shift towards the red of the BCs of the He I profiles.

He I λ5876 to He I λ6678 line ratios give an indication of the physical conditions where they are formed. At low densities the triplet to singlet line ratio is around 3.5. Initially, as density increases so does this ratio. However, at high enough densities the line ratio starts to decrease, approaching values near unity (see BEK01 and references therein). We determined line fluxes in the He I lines by combining the IDS high resolution data, from which we computed the equivalent widths of the narrow and broad components, with the low resolution flux-calibrated spectra, from which we determined the continuum flux in the vicinity of the lines. Results are shown in Table 5. Uncertainties in the line ratios were estimated from the uncertainties in the determination of the continuum level near the emission line, from the low resolution data and from the formal uncertainties that result to the equivalent widths from Gaussian fitting.

In general, the line ratios are larger for BC than for NC, as expected if the region in which the BC originates is of lower density than that where the NC arises. However, with the exception of JD 2449318.6, the NC ratios are significantly higher than the average in BEK01. This indicates that, during the period of time discussed here,

Table 5. Narrow and broad component He I 5876 to He I 6678 Å line ratios.

JD	2449318.6	2449320.4	2449321.4	2449322.5
NC	1.8 ± 0.1	3.7 ± 0.2	2.7 ± 0.1	3.2 ± 0.1
BC	4.3 ± 0.1	2.5 ± 0.1	3.6 ± 0.2	4.2 ± 0.2

densities in LkHα 264's NC formation region are generally lower than those in the corresponding region of the average T Tauri star.

3.3.3. O I inverse P Cygni profiles

The high resolution echelle spectrum taken on the night of October 19 1999 allowed us to obtain line profiles which contain kinematic information that can be used to understand mass flows in the stellar atmosphere. We find spectroscopic evidence for the presence of stellar winds from blueshifted absorption in several emission lines. Inverse P Cygni profiles in two lines, O I λ7773 and O I λ8446 (Fig. 10) reveal the presence of infalling material. The O I λ7773 line profile shown here is the residual normalised line profile, i.e. the photospheric contribution has been removed by subtracting a K3 V template. The O I λ8446 line profile did not have the photospheric contribution removed since we do not have the spectrum of the template around that wavelength region. The absorption features observed near -720 km s^{-1}, -420 km s^{-1} and $+750$ km s^{-1} are photospheric in origin, corresponding respectively to TiI lines at 8426.5, 8434.9 and 8435.6 Å and to the 8468.4 Å Fe I line.

The centre of the redshifted absorption features lie near $+250$ km s^{-1}, while their widths are about 300 km s^{-1} at the continuum level. The absorptions meet the continuum in the red slightly above $+400$ km s^{-1}. These velocities are consistent with infall from a height of a few stellar radii for typical T Tauri stars' parameters (Edwards et al. 1994). These line profiles indicate that infall was occurring when the spectra was acquired.

4. Differential photometry

The observed field containing LkHα 264 was chosen so as to also include stars bright enough to be used as reference for differential photometry. The chosen field contains five such stars (henceforth referred to as field stars), about which not much information exist other than their approximate magnitudes from the USNO Catalogue (as consulted at ESO with GAIA). After examining the differential photometry of the various field stars against each other we decided to choose three of them to serve as reference for LkHα 264. A virtual reference star was constructed for each night by averaging the instrumental magnitudes of the three chosen field stars. LkHα 264's differential photometry was computed relative to the virtual reference star. Results are shown in Fig. 11 where independent data points are displayed between 0 and 2π. An estimate of the uncertainty in each data point is given by

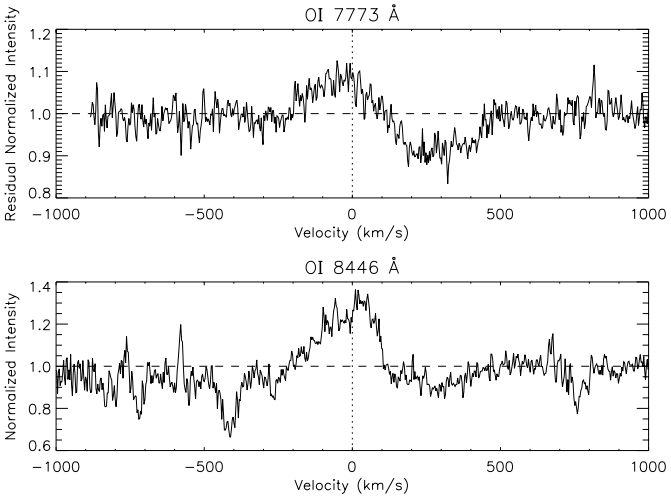

Fig. 10. Top panel: residual normalised O I λ7773 line profile. Bottom panel: normalised O I λ8446 line profile. Velocities are referenced to the star's rest frame.

the standard deviation of the nightly sequence of differential magnitudes of the three field stars, which amounts to 0.01 at g' and 0.02 at r'. These uncertainties, smaller than the symbol size in Fig. 11, dominate those that result from Poissonian statistics in determining the instrumental magnitudes.

LkHα 264 show variability in both g'- and r'-bands. As commonly observed in T Tauri stars, the amplitude of the variation is higher in the blue than in the red. At the g'-band, the star's brightness varies by about 0.6 mag between maximum and minimum intensity whereas the same variation at the r'-band is about 0.2 mag. Variations in both bands seem to occur nearly in phase, with no hint for a significant relative shift in time between the g'- and r'-band light curves.

5. Discussion

The data presented here allow us to identify different types of variability in LkHα 264: variations in the continuum level characterised by different amplitudes, variations in the continuum dependency with wavelength, variations in emission line fluxes and line profile variability. The timescales in which such variations occur also seem to be diverse.

Variability in TTS is usually explained by rotational modulation by cool or hot spots, by variable accretion, by chromospheric activity or by inhomogeneous circumstellar envelopes (e.g. Appenzeller & Mundt 1989).

Inhomogeneous circumstellar envelopes are unlikely to be the cause for most of the observed variations in the continuum flux described here. Extinction would decrease and redden the stellar flux but it would produce no veiling effect. The correlation found between the variations in the observed veiling and variations in the observed continuum flux (Fig. 4), is a strong indication that the cause

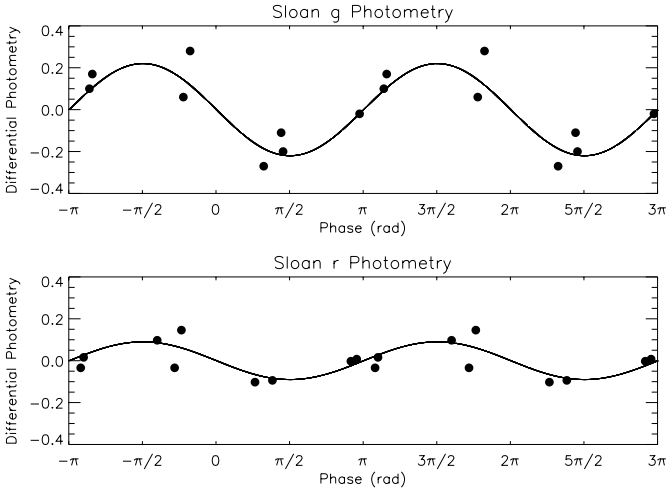

Fig. 11. Differential photometry. Differential magnitudes were normalised to zero by subtracting their average value. The lines represent best fit periodical solutions to the data (period 3.04 days – see Sect. 5.1). The data is represented in a phase diagram corresponding to the above period.

of continuum variability is an extra continuum source that veils the stellar photospheric spectrum.

5.1. Rotational modulation and hot spots

Rotational modulation of LkHα 264 brightness is far from being well established. Mendoza et al. (1990) performed Strömgren photometry for this star during eleven consecutive nights in October/November 1986. Their study shows no signs of periodic behaviour. Fernandez & Eiroa (1996) suggest a rotation period near 2.6 days (August 1991 data), but their photometric data suffer from inadequate time sampling. The differential photometry presented here suffers from the same problem. We tentatively fit a simple periodic solution to our observations. A Lomb Periodogram analysis yields a period of 3.04 days but with very modest false alarm probabilities, respectively 0.42 and 0.65 for g' and r'. Given the above period, a linear least squares fit for the amplitudes and phases was performed. We found amplitudes of 0.22 at g' and 0.09 at r' with the variations occurring very nearly in phase in the two wavebands. We plot that solution in the phase diagram in Fig. 11. We note that such a period is consistent with that of the periodical variations found by Gameiro et al. (1993) in the behaviour of the He I and Na D emission lines. A better time sampling is necessary if such a period is to be confirmed.

Periodic variations in TTS are interpreted as being due to the presence of hot or cool spots in the star's surface. Fernandez & Eiroa (1996) model their photometric observations with a hot spot with temperatures in the range 4600–6400 K and covering factors between approximately 37% and 2%. While we cannot make a similar analysis with our photometric data (we only have differential photometry for g' and r'), the fact that the amplitude of the variations in the g'-band is roughly double that observed in the r'-band hints that if they are due to the presence of a spot it is most likely a hot spot.

In Costa et al. (1999) the observed UV spectrum and the JD 2449322.54 optical spectrum of LkHα 264 are fitted with the sum of three components: a stellar black-body at 4300 K, hydrogen free-free plus free-bound emission at 3.5×10^4 K (that dominates continuum emission only in the UV at wavelengths shorter than 2000 Å) and an extra black-body at 8700 K covering 4% of the stellar surface, all subject to a Savage & Mathis (1979) extinction law with $A_V = 0.8$. The latter black-body component can be interpreted as a hot spot on the star's surface. If we replace the above stellar black-body contribution by the photospheric contribution discussed in Sect. 5.1, we explain the excess emission of the JD 2449322.54 spectrum by adding a contribution from a 8700 K black-body covering 6% of the stellar surface (see Fig. 2), in tune with the results from Paper I. The excess continuum emission from the remaining nights could not be fitted by black-body emission. The excess spectrum beyond around 5500 Å falls much faster than a black-body does. By assuming a very low extinction ($A_V < 0.1$) one can reproduce the slopes observed in the excess spectra of those nights. However, decreasing the extinction to such values would lead to a substantial increase in the observed flux, which goes against the observations: the steepest excess spectra correspond to the fainter states of LkHα 264.

To compare the variations observed in the low resolution spectroscopy with those observed photometrically we performed g' and r' synthetic photometry on the flux calibrated spectra. The results show that variations during the November 1993 run are within 0.2 mag for g' and 0.1 mag for r', except for the night of JD 2449322.54, when LkHα 264 was 0.61 mag brighter than average in g' and 0.57 mag brighter than average in r'. Hence, the November 1993 variations seem to be similar to those observed during 1999, with the exception of that of JD 2449322.54, which probably corresponds to an exceptional event.

5.2. Line profiles: Probing the dynamics

Hot spots in T Tauri stars are usually thought to result from a shock, as accretion flows hit the stellar photosphere. Evidence for accretion in LkHα 264 has never been clearly established from a dynamical point of view. While one could argue that the observed profiles of Hα and Hβ display characteristics that are typical of those produced by magnetospheric accretion models, such as being centrally peaked, slightly blueshifted and with blue to red asymmetry factors slightly larger than one (Hartmann et al. 1994; Edwards et al. 1994; Muzerolle et al. 1998), unequivocal model-independent evidence for accretion comes only from the presence in the line profiles of redshifted absorption falling bellow the continuum. We could find no record of emission lines in spectra of LkHα 264 with such a characteristic until now. The O I line profiles we present

here seem to be the first clear model-independent indication that LkHα 264 is actively accreting (recall Fig. 10).

When the O I observations were obtained (19 October 1999) the star did not seem to be in a particularly active state. For that date, the amount of veiling computed at 5870 Å is 0.31 ± 0.03. Such a value corresponds to the typical amount of excess emission found in LkHα 264, not to the exceptionally high state observed on JD 2449322.54 (see Fig. 3). In addition, the He I 5876 Å and the He I 6678 Å lines observed then, lack the broad component clearly identified during the 1993 campaign (see Fig. 8 for a comparison between the 1999 He I 5876 Å profile and a corresponding 1993 profile).

BEK01 analyse the helium emission from a sample of 31 CTTS and propose a dual origin for the broad component: magnetospheric infall and/or a hot wind. BC line centres occurring at redshifted velocities larger than 8 km s^{-1} are indicative of origin in funnel accretion flow, whereas BC with line centres blueshifted by more than 30 km s^{-1} likely arise in a hot wind. Furthermore, they suggest that when a hot wind is present, the luminosity and temperature of the accretion shock seems to decrease. Our Lkhα 264 observations reveal that when the continuum level is around its average value (lowish excess emission) the BC in the He I λ5876 is blueshifted by more than 30 km s^{-1}. On the other hand, when the continuum level is high (larger excess emission), the He I λ5876 BC is slightly redshifted or centred very near the star's rest velocity (recall Fig. 9). The shift towards the red of the He I lines is accompanied by a similar shift in the Na D lines. The latter were blueshifted by nearly 70 km s^{-1} in November 26 and redshifted by nearly 10 km s^{-1} in November 30. These similar shifts suggest that both lines could be formed in a common region. Such an idea had already been suggested by Lago & Gameiro (1998), as the result of the strong correlation between Na D and He I λ5876 equivalent widths observed during two runs in 1990 and 1993. The main contributor for the total equivalent width of the He I lines is the BC. The He I vs. Na D correlation we find is in fact between the He I λ5876 BC and Na D lines (we found a linear correlation of 0.83). There is no clear correlation with the narrow component (linear correlation of 0.48). A similar result is found when comparing the behaviour of both components of He I λ6678 with Na D, although in this case the correlation is not as high (we determined a correlation of 0.70 for the broad component and no correlation with the narrow component).

In addition, the presence of a wind during the nights of 1993 November 28 and 29 is revealed by the Na D and Hα line profiles (see Figs. 3 and 7 in Lago & Gameiro 1998) which, for those nights, display a narrow absorption blueshifted by about 120 km s^{-1}.

During the November 1993 run, the hot wind seemed stronger on the night of the 28th (largest equivalent width of the He I blueshifted broad component). Emission line fluxes observed that night are, in general, larger than those observed in the remaining "quiet" nights. On the other hand, in October 1999, when we see no BC in the

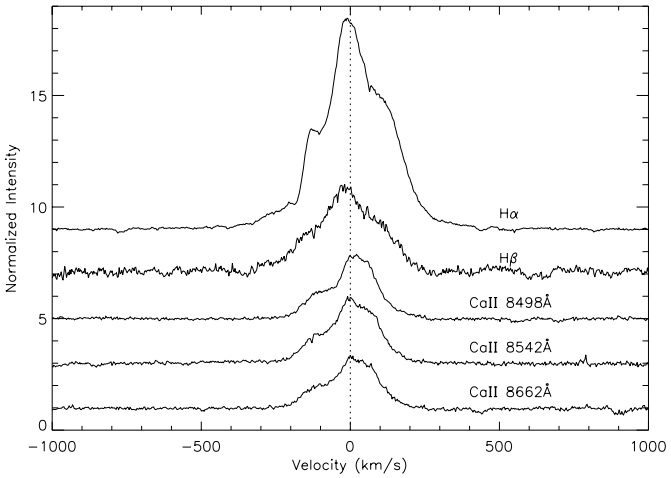

Fig. 12. 19 October 1999 Hα, Hβ and infrared CaII triplet line profiles. Profiles are shifted vertically for clarity. The velocity scale is referred to the stellar rest frame.

He I lines, all emission lines are relatively faint. This correlation between the strength/absence of a hot wind and the amount of flux in the emission lines seems to indicate that a hot wind provides a significant contribution towards both hydrogenic and metallic line emission.

In the BEK01 picture, the lack of a BC on the October 1999 profile indicates that, at that particular date, a hot wind is not present nor is the accretion flow hot enough to produce emission in the He I lines. Despite the lack of this signature for a hot wind, a cooler wind (cooler than that traced by He I in emission) still seems to be present in Lkhα 264. The Hα, Hβ and infrared CaII triplet line profiles all provide indications for such wind (see Fig. 12). In all these lines there is a clear asymmetry in the blue wing of the emission profile, between -100 and -130 km s^{-1}, indicative of outflowing material.

Apart from the blueshifted asymmetries, all five line profiles also display asymmetries redward of the line centre. These asymmetries are very probably related to the accretion flow, so clearly identified in O I, showing that these lines have contributions from distinct regions around LkHα 264.

5.3. Continuum emission vs. line profiles/fluxes

Are the changes observed in the line profiles discussed above related to the variability in the continuum emission?

The anomously high continuum level observed on JD 2449322.54 is definitely accompanied by a shift towards the red of the He I BCs. If the shift is the result of changing the dominant source of He I emission from the wind to the accretion flow, as suggested by the BEK01 scenario, the increase in continuum brightness is probably associated with an increase in the accretion rate. On the other hand, when the continuum flux is minimum (JD 2449321.36), the BC of the He I lines is blueshifted and has its largest equivalent width. In terms of the BEK01 scenario, when

a hot wind is present the star seems to show a lower continuum brightness.

The variations in continuum and line fluxes show two types of behaviour (compare Figs. 6 and 7). At times, variations in the line fluxes seem directly correlated to variations in the continuum intensity, e.g. the night of November 30 when both continuum and lines increase significantly in brightness. However, an increase in the line fluxes can also occur together with a decrease in continuum intensity, as observed for the night of November 28, or a substantial decrease in line fluxes occurring when the continuum stays roughly constant (e.g. October 1999 observations). Variations in line emission seem to occur a lot more easily than variations in the continuum.

The flux variations of lines is strongly correlated even when we compare lines with very different excitation potentials such as the Fe II (∼3 eV) and the hydrogen Balmer lines (∼10–13 eV), with only a few exception, such as Hα (Table 4).

5.4. Flaring activity vs. accretion

Optical flares have been reported both in WTTS and in CTTS (e.g. Gham 1990; Guenther & Ball 1999). They are characterised by a rapid increase (typically <1 hour) and a slower decay (up to a few hours from maximum to half-peak luminosity) of their brightness and Hβ and Hγ line emission. The exceptional increase in brightness observed on JD 2449322.54 could, in principle, be due to a flare like event. Our data lacks the time sampling resolution to evaluate such hypothesis. By analysing the change in the continuum shape that accompanied the event and the variation in line fluxes alone, we are not able to conclusively distinguish between a flare and enhanced accretion. However, we note that although the Hβ and Hγ emission line fluxes increase from the November 29 to November 30 by a factor of ∼1.6, the continuum flux and veiling also increase between these two nights. We recall that optical veiling is generally interpreted as the result of excess emission from an accretion shock. The flare event observed in the CTTS FN Tau by Guenther & Ball (1999) is characterised by a clear increase in the Hβ and Hγ EWs while the veiling and continuum flux remain constant, hinting that the JD 2449322.54 event might not be associated with a flare but with variable accretion.

5.5. Comparison with model predictions

The observations discussed here mostly pertain to line emission and the spectrum of the derived excess emission. These can be directly compared with model predictions for line profiles (Muzerolle et al. 2001) within the now widely accepted magnetospheric accretion paradigm, and with predictions for the continuum excess emission from studies of the structure and emission of the accretion shock in T Tauri stars CG98.

5.5.1. Line profiles

Muzerolle et al. (2001) produced a grid of line profiles for Hα, Hβ, Hγ, Paβ, Brγ and Na D1 and D2 covering four accretion rates (log $\dot{M}(M_\odot/\mathrm{yr}) = -6$, -7, -8 and -9), five maximum values for the temperature distribution (6, 7, 8, 9 and 12 thousand K), four inclination angles ($i = 10^\mathrm{o}$, 30^o, 60^o and 75^o) and four magnetospheric sizes (small and wide, small and narrow, large and wide and large and narrow)[2]. The model results for Hα and Hβ were compared with the observed profiles obtained on 19 October 1999, i.e. those in Fig. 12. A reasonably good match between model and observed Hβ profiles, as judged by eye, results only from two sets of parameters: log $\dot{M}(M_\odot/\mathrm{yr}) = -6$, $T_\mathrm{max} = 7000$ K, $i = 30^\mathrm{o}$ in a small wide magnetosphere (hereafter set 1) and log $\dot{M}(M_\odot/\mathrm{yr}) = -7$, $T_\mathrm{max} = 8000$ K, $i = 60^\mathrm{o}$ again in small wide magnetosphere (hereafter set 2). However, when the Hα model profiles that result from these two parameter sets are compared with the observed one, the discrepancy is clear. Both model Hα profiles are too wide and too faint. We note that Hα and Hβ were observed simultaneously in a single echelle spectrum. Searching through all the Hα profiles in the model grid reveals that qualitatively many model profiles are similar to that observed. However, a quantitative comparison shows clear differences, both in the width and in the strength of the qualitatively similar line profiles.

In addition to Hα and Hβ profiles, the echelle spectrum shows that at that date there is no significant emission from the Na D1 and D2 lines (observed Na D1 and D2 not shown here). What are the predicted Na D1 and D2 profiles for parameter sets 1 and 2? Set 1 predicts profiles with a peak intensity (normalized to the continuum) above 3.5. Set 2 predicts profiles with a peak slightly above 1.3, in the same units, and a clear redshifted absorption feature. Neither of these resemble the observations.

The lack of agreement between the model and the observed line profiles hints that either LkHα 264 has an accretion geometry and/or physical conditions in its accretion flow that depart significantly from the treatment used by Muzerolle et al. (2001), or that the accretion flow is not the only contributor to line emission.

5.5.2. Excess continuum emission

CG98 compute the emergent flux from accretion column models in the context of T Tauri stars. The emergent flux resulting from the models presented in that work (their Fig. 4) can be readily compared to the excess emission flux presented in our Fig. 2. In order to better compare the model predictions with our observations we digitized the solid lines of CG98's Fig. 4.

[2] The grid of line profile models is available electronically as ascii files, each with two columns tables, at `cfa-www.harvard.edu/cfa/youngstars` in the "Publications" link.

The shape of the stronger excess emission spectrum (uppermost spectrum in Fig. 2) can be successfully matched, as judged by eye, by the log $\mathcal{F} = 11.5$ model reddened by A_V between 0.2 and 0.9 or by the log $\mathcal{F} = 11$ model with $A_V = 0$. CG98 show that the dependence of the model results in the mass over radius ratio is weak, hence we do not consider such variations here. The amount of reddening necessary for a match between the log $\mathcal{F} = 11.5$ and the observations is in general agreement with the A_Vs found in the literature for LkHα 264 ($A_V = 0.5$ in Cohen & Kuhi 1979 and $A_V = 0.8$ in Costa et al. 1999 and Luhman 2001). The $A_V = 0$ necessary for a match of the model with log $\mathcal{F} = 11$ is probably unrealistic. If one uses a stellar radius of 2 $R_\odot$, typical of T Tauri stars, and a distance of 65 pc (Hobbs 1986) the above models predict the observed amount of excess emission for filling factors of around 0.4%. This is in good agreement with the filling factors found by CG98 for the less veiled T Tauri stars in their studied sample, but roughly a factor of 10 smaller than that that results from the black body interpretation alluded to in Sect. 5.1. If instead we use 275 pc (Luhman 2001) the filling factor becomes around 6%, comparable to that derived by the black-body approach.

We were unable to achieve a reasonable match between the CG98 models and the shape of the excess emission for the lower excess emission states of LkHα 264 (lower two spectra in Fig. 2 and veiling in Fig. 5). The shape of the model predictions is too flat when compared to the observations, even for $A_V = 0$. Increasing the amount of extinction affecting the predicted model excess makes the problem worse, since it flattens the shape of the spectrum even further. The sharp drop in continuum emission, occurring just before 5500 Å, observed for the lower excess emission states (Fig. 2), is the cause for the model mismatch. Interestingly, we note that the presence of a similar drop in the excess emission continuum of the stars modelled by CG98 would not be apparent, since the wavelength coverage in their observed spectra stops at 5300 Å.

The veiling measurements displayed in Fig. 5 show the same sort of decrease in excess emission. Comparing the observed veiling with that predicted by CG98 (their Fig. 11) shows, as expected from the considerations above, model veilings decreasing too slowly (we corrected the predicted veiling from a K7-M0 to a K5 photosphere). In addition, the veiling resulting from the models decrease monotonically all the way to the near infrared (NIR) part of the spectrum. Figure 5 shows an increase in the amount of veiling in the very red end of the spectrum, in line with the results obtained by Folha & Emerson (1999), who find higher than expected NIR veiling.

Our comparison between model and observed excess emission spectra is limited to the results shown in Fig. 4 of CG98. A full exploration of the model parameter space would be desirable in order to understand whether continuum excess emission from accretion funnels is capable of explaining the observations discussed here, and in particular the change in continuum slope observed to occur near 5500 Å.

6. Conclusions

The hypothesis that the origin of the observed variability in LkHα 264 is extrinsic is not supported by the data presented here. Variations with causes such as variable circumstellar extinction would not produce a tight correlation between observed intensity and measured veiling.

Typical variations can be produced by the presence of inhomogeneities on the stellar surface and rotational modulation. If that is the case, unless the lifetime of such inhomogeneities is very small (one or two days), a photometric period still needs to be unambiguously identified.

O I line profiles reveal the presence of an accretion flow onto the star. Such flow would produce one or more hot spots as infalling material shocks near the stellar surface.

The November 1993 He I profiles indicate the presence of a hot wind at that time. The October 99 data show no signs for the presence of a hot wind (no BC in He I emission lines). However a cooler wind at the latter date is revealed by Balmer and CaII infrared triplet line profiles. Emission lines fluxes in October 1999 are considerably smaller than those observed in November 1993, despite the identical continuum intensity. A hot wind seems to contribute significantly to emission in both hydrogen and metal lines. The lack of success in explaining the Hα, Hβ and Na D lines within the context of magnetospheric accretion, reinforces the idea that other line emission sources are at play on LkHα 264.

The exceptional activity registered during the night JD 2449322.54 may correspond to an increase in LkHα 264's accretion rate or to a flare-like event. Distinguishing between the two interpretations seems impossible given the available data. A better time sampling during the event would have to have happened in order to clearly distinguish between these two possibilities. Nevertheless, the discussion in Sect. 5 hints for variable accretion as the cause of the observed changes.

Accretion models are successful in explaining the continuum excess emission observed during the night of JD 2449322.54 but not the continuum slope observed during the other nights for which we have observations. These conclusions are based on the published model results only. A more complete exploration of the model parameter space is necessary to assess this matter fully.

LkHα 264 is a CTTS displaying different types of activity. The presence of infalling matter, hot and cool outflows and the possibility of enhanced solar like activity such as flares, make it an excellent target for studying how these different phenomena are related. Such knowledge is essential if one is to better understand T Tauri stellar systems, i.e. if one is to better understand how the young Sun behaved. Synoptic observations on timescales ranging from minutes to hours to days are the only way to achieve that goal.

Acknowledgements. We thank Dr. Nicholas Walton for donating about 10 min per night during his JKT Supernovae programme to the photometric observations reported here. We thank Javier Mendez and Guillaume Blanc for executing those observations. We also thank an anonymous referee for valuable comments that helped to improve this paper. D. F. M. Folha aknowledges financial support from the "Subprograma Ciência e Tecnologia do 2º Quadro Comunitário de Apoio". This work is supported by Fundação para a Ciência e Tecnologia, under project POCTI/1999/Fis/34549.

References

Appenzeller, I., & Mundt, R. 1989, A&ARv, 1, 291
Basri, G., & Bertout, C. 1989, ApJ, 341, 340
Beristain, G., Edwards, S., & Kwan, J. 2001, ApJ, 551, 1037 (BEK01)
Bertout, C., Basri, G., & Bouvier, J. 1988, ApJ, 330, 350
Batalha, C. C., Stout-Batalha, N. M., Basri, G., & Terra, M. A. O. 1996, ApJS, 103, 211
Calvet, N., & Gullbring, E. 1998, ApJ, 509, 802 (CG98)
Camenzind, M. 1990, Rev. Mod. Astron., 3, 234
Cardelli, J. A., Clayton, G. C., & Mathis, J. S. 1989, ApJ, 345, 245
Cohen, M., & Kuhi, L. V. 1979, ApJS, 41, 743
Costa, V. M., Gameiro, J. F., & Lago, M. T. V. T. 1999, MNRAS, 307, L23
Edwards, S., Hartigan, P., Ghandour, L., & Andrulis, C. 1994, AJ, 108, 1056
Fernández, M., & Eiroa, C. 1996, A&A, 310, 143
Folha, D. F. M., & Emerson, J. P. 1999, A&A, 352, 517
Gahm, G. F. 1990, Flare stars in star clusters, associations and the solar vicinity, in Proceedings of the 137th IAU Symposium, Byurakan, Armenian SSR 1989 (Kluwer Academic Publishers, The Netherlands), 193
Gameiro, J. F., Lago, M. T. V. T., Lima, N. M., & Cameron, A. C. 1993, MNRAS, 261, 11
Guenther, E., & Ball, M. 1999, A&A, 347, 508
Gullbring, E., Hartmann, L., Briceno, C., & Calvet, N. 1998, ApJ, 492, 323
Gullbring, E., Calvet, N., Muzerolle, J., & Hartmann, L. 2000, ApJ, 544, 927
Hamann, F., & Persson, S. E. 1992, ApJS, 82, 247
Hartigan, P., Hartmann, L., Kenyon, S., Hewett, R., & Stauffer, J. 1989, ApJS, 70, 899
Hartmann, L., Hewett, R., & Calvet, N. 1994, ApJ, 426, 669
Herbig, G. H., & Bell, K. 1988, Lick Obs. Bull., 1111
Hobbs, L. M., Blitz, L., & Magnani, L. 1986, ApJ, 306, L109
Jayawardhana, R., Wolk, S. J., Barrado, Y., et al. 2001, ApJ, 550, L197
Joy, A. H. 1945, ApJ, 102, 168
Kenyon, S. J., Gomez, M., Marzke, R. O., & Hartmann, L. 1994, AJ, 108, 251
Königl, A. 1991, ApJ, 370, L39
Lago, M. T. V. T., & Gameiro, J. F. 1998, MNRAS, 294, 272
Luhman, K. L. 2001, ApJ, 560, 287
Lynden-Bell, D., & Pringle, J. E. 1974, MNRAS, 168, 603
Savage, D. B., & Mathis, J. S. 1979, ARA&A, 17, 73
Mendoza, E. E., Rolland, A., & Rodíguez, E. 1990, A&AS, 84, 29
Meyer, M. R., Calvet, N., & Hillenbrand, L. A. 1997, AJ, 114, 288
Muzerolle, J., Calvet, N., & Hartmann, L. 1998, ApJ, 492, 743
Muzerolle, J., Calvet, N., & Hartmann, L. 2001, ApJ, 550, 944
Pearson, K. J., & King, A. R. 1995, MNRAS, 276, 1303
Pickles, A. J. 1998, PASP, 110, 863
Pound, M. W. 1996, ApJ, 457, L35
Shu, F., Najita, J., Ostriker, E., et al. 1994, ApJ, 429, 781
Valenti, J. A., Basri, G., & Johns, C. M. 1993, AJ, 106, 2024